Title	The effect of remodelling and contractility of the actin cytoskeleton on the shear resistance of single cells: a computational and experimental investigation
Author(s)	Dowling, Enda P.; Ronan, William; Ofek, Gidon; Deshpande, Vikram S.; McMeeking, Robert M.; Athanasiou, Kyriacos A.
Publication Date	2012-07-18
Publication Information	Dowling, Enda P., Ronan, William, Ofek, Gidon, Deshpande, Vikram S., McMeeking, Robert M., Athanasiou, Kyriacos A., & McGarry, J. Patrick. (2012). The effect of remodelling and contractility of the actin cytoskeleton on the shear resistance of single cells: a computational and experimental investigation. Journal of The Royal Society Interface, 9(77), 3469-3479. doi: 10.1098/rsif.2012.0428
Publisher	The Royal Society Publishing
Link to publisher's version	http:/dx.doi.org/10.1098/rsif.2012.0428
Item record	http://hdl.handle.net/10379/5939
DOI	http://dx.doi.org/10.1098/rsif.2012.0428

The effect of remodelling and contractility of the actin cytoskeleton on the shear resistance of single cells: A computational and experimental investigation

Enda P. Dowling[1], William Ronan[1], Gidon Ofek[2], Vikram S. Deshpande[3], Robert M. McMeeking[4], Kyriacos A. Athanasiou[5], J. Patrick McGarry[1,*]

[1]Mechanical and Biomedical Engineering, National University of Ireland, Galway, University Road, Galway, Ireland
[2]Department of Bioengineering, Rice University, 6500 Main Street, Houston, TX-77030, USA
[3]Department of Engineering, University of Cambridge, Trumpington Street, Cambridge CB2-1PZ, UK
[4]Department of Mechanical Engineering and Department of Materials, University of California, Santa Barbara, CA-93106, USA
[5]Department of Biomedical Engineering, University of California, Davis, One Shields Ave., Davis, CA-95616, USA

[*]Author for correspondence (patrick.mcgarry@nuigalway.ie)

Summary

The biomechanisms which govern the response of chondrocytes to mechanical stimuli are poorly understood. In the current study a series of *in vitro* tests are performed in which single chondrocytes are subjected to shear deformation by a horizontally moving probe. Dramatically different probe force-indentation curves are obtained for untreated cells and for cells in which the actin cytoskeleton has been disrupted. Untreated cells exhibit a rapid increase in force upon probe contact followed by yielding behaviour. Cells in which the contractile actin cytoskeleton was removed exhibit a linear force-indentation response. In order to investigate the mechanisms underlying this behaviour, a 3D active modelling framework incorporating stress fibre remodelling and contractility is used to simulate the *in vitro* tests. Simulations reveal that the characteristic force-indentation curve observed for untreated chondrocytes occurs due to two factors: (i) yielding of stress fibres due to stretching of the cytoplasm near the probe; (ii) dissociation of stress fibres due to reduced cytoplasm tension at the front of the cell. In contrast, a passive hyperelastic model predicts a linear force-indentation curve similar to that observed for cells in which the actin cytoskeleton has been disrupted. This combined modelling-experimental study offers a novel insight into the role of the active contractility and remodelling of the actin cytoskeleton in the response of chondrocytes to mechanical loading.

Keywords: cell mechanics; actin cytoskeleton; cell contractility; chondrocyte; finite element; *in vitro* shear.

Short Title: Actin contractility during cell shear

Introduction

Numerous *in vitro* studies have demonstrated that chondrocytes react to mechanical stimuli. Compression of chondrocytes in agarose gel induces disruption of the actin cytoskeleton [1, 2]. In addition, static compression has been shown to downregulate type II collagen expression in chondrocytes [3], while cyclic compression restores levels to those of unperturbed cells [4]. Chondrocytes cultured in a monolayer show decreases in chondrogenic gene expression, while inhibition of actin polymerisation causes an increase in type II collagen and glycosaminoglycan production [5]. Furthermore, disruption of the actin cytoskeleton alters the biomechanical response of chondrocytes to micropipette aspiration [6] and compression [7]. Despite such extensive *in vitro* investigation, the mechanisms by which chondrocytes actively respond to mechanical loading are not well understood.

Previous studies have investigated the effect of shear deformation in cartilage tissue during joint movement [8, 9]. It has been demonstrated that elevated shear strains are found in cartilage containing focal defects, suggesting that those strains contribute to the further deterioration of the tissue [10]. Previous *in vitro* studies have shown that shear directly affects chondrocyte morphology [11] and metabolism [12]. Huang et al. [13] have shown that as chondrocytes spread with the actin cytoskeleton reorganising at the cell periphery, the cells become more resistant to shear forces. Clearly, shear loading in cartilage is important to investigate. Understanding the role of the actin cytoskeleton in the response of chondrocytes to shear loading may help to elucidate the biomechanisms involved in cartilage regeneration or degeneration.

Finite element modelling has previously been used to characterise the mechanical properties of chondrocytes to mechanical stimuli. Ofek et al. [14] modelled the response of single chondrocytes to compression using an elastic model. Viscoelastic models have been employed to simulate the response of chondrocytes to micropipette aspiration [15, 16]. McGarry and McHugh [17] assumed a viscoelastic material formulation for the chondrocyte cytoplasm and nucleus to simulate the *in vitro* detachment of chondrocytes due to probe indentation [13]. This computational study highlights the shortcoming of passive viscoelastic cell models by demonstrating that the cell stiffness must be artificially increased as cells spread in order to replicate experimental measurements [13]. A similar deficiency has been reported for the passive modelling of parallel plate compression of cells [18]. The use of such passive material models ignore the key mechanisms by which cells actively respond to mechanical stimuli, and hence offer a limited insight or predictive capability. An active modelling framework proposed by Deshpande et al. [19], which incorporates the biomechanisms underlying the formation, dissociation and contractility of the actin cytoskeleton has been shown to accurately predict changes in cell contractility as a function of cell area and substrate stiffness [20] for a range of cell phenotypes seeded on micro-pillar arrays. Most recently, this formulation has been shown to accurately predict the increased compressive resistance of spread cells compared to round cells [21]. In the current study, this formulation is used to demonstrate the important active role of the actin cytoskeleton in the response of chondrocytes to applied shear loading.

The objective of the current work is to investigate the role of the active remodelling and contractility of the actin cytoskeleton in the response of chondrocytes to mechanical deformation. Specifically, *in vitro* experiments are performed in which the resistance of single chondrocytes to applied shear deformation is observed. Additionally, tests are also performed on chondrocytes in which the contractile actin cytoskeleton has been disrupted. It is hypothesised that commonly used passive hyperelastic models cannot reproduce the experimentally observed behaviour. An active bio-chemo-mechanical model based on stress fibre (SF) evolution and contractility is implemented in order to simulate our *in vitro* shear

experiments. It is demonstrated that the active remodelling and contractility of the actin cytoskeleton is the biomechanism governing the response of chondrocytes to shear.

Materials and Methods

Experimental Methods

Articular cartilage was harvested from bovine tissue and single chondrocytes were isolated from the middle/deep zones of the tissue. The cells were seeded in baseline media on glass substrates and incubated for 3 hours. The glass substrate containing the cells was then placed in a petri dish on an inverted microscope. A shear deformation was applied to individual cells by a tungsten probe [22]. Initially, the probe was positioned adjacent to the cell, 4μm above the substrate (figure 1*a*). The fixed (top) end of the probe was then moved horizontally towards the cell at a constant speed of 4μm/s. The free (bottom) end of the probe indents the cell, leading to a shear deformation (figure 1*b*). Due to the resistance of the cell to deformation, a deflection is imparted on the free end of the probe relative to the known position of the fixed end. Using simple beam theory, this deflection (δ) is used to determine the force required to deform the cell throughout the shear experiment. In order to monitor the deformed cell geometry and the probe deflection, a video camera was connected to the microscope (figure 1*c* and *d*). Individual frames were analysed using image analysis software. Five separate cells were fixed at maximum shear deformation and stained using phalloidin antibodies to observe alterations in the actin cytoskeleton. An additional series of shear experiments was carried out on cells where one of the three following cytoskeletal components was disrupted: actin filaments, intermediate filaments, and microtubules. A detailed description of the experimental methods is provided in Appendix A of the Electronic Supplementary Material. Probe force-indentation curves were generated for all experimental groups, in order to measure the contribution of the cytoskeleton components in the response of chondrocytes to shear. Probe indentation is defined as the forward-most position of the probe minus the back edge position of the cell.

Computational Methods

Theoretical Framework for Active Stress Fibre Remodelling and Contractility

The actin cytoskeleton provides the active machinery by which cells generate forces. It consists of SFs, which are comprised of actin filaments and the motor protein myosin. Contractile forces are generated via a cross-bridge cycling process, similar to that observed for skeletal muscle, whereby the hydrolysis of ATP causes the myosin head to pivot and exert traction on the attached actin filament. Regarding the remodelling of the actin cytoskeleton, two key observations should be noted: (i) SFs assemble due to a signalling cascade (such as RhoA/Ca^{2+}) in the cell [23]; (ii) SFs dissociate due to a reduction in tension in the cell cytoplasm [23]. From these two observations, a first order kinetic equation has been proposed [19] that describes the remodelling of the actin cytoskeleton:

$$\frac{d\eta}{dt} = [1-\eta]\frac{Ck_f}{\theta} - \left[1-\frac{T}{T_0}\right]\frac{\eta k_b}{\theta} \tag{1}$$

where η is the non-dimensional SF activation level. The first term on the right hand side describes the rate of formation of SFs in response to a signal C. The second term on the right hand side describes the rate of dissociation of SFs when the tension in the fibre drops below the isometric tension T_o. θ is a constant that controls the decay rate of an activation signal. k_f and k_b are reaction rate constants.

The complete model of contractility and remodelling of SFs is depicted in figure 2*a-d*. As shown in figure 2*a*, an exponentially decaying signal $C = \exp(-t/\theta)$ (as observed for

chondrocytes [24]) leads to the formation of a contractile SF bundle. If the SF is fully activated (η = 1), it will produce a maximum isometric tension T_{max}. If the SF shortens, due to its own active contractility or due to an externally applied load, its tension-velocity relationship is based on the classical cross-bridge cycling model developed for actin-myosin interactions in skeletal muscle [25], whereby the SF produces lower tension when the shortening velocity is large (figure 2*b*). When the fibre lengthens, for example upon the application of an external load, it yields, producing a tension equal to the isometric tension for all lengthening velocities. Finally, as shown in figure 2*c*, when the SF shortens, the associated reduction in tension (Eq. 1) leads to dissociation of the SF, thus lowering the activation level η. This in turn lowers the SF contractility with the reduced isometric tension given as $T_o=\eta T_{max}$, as illustrated by the altered tension velocity relationship (blue dashed curve, figure 2*b*). The Hill-like [25] equation used to model the contractility of SFs is specified as:

$$\frac{T}{T_0} = \begin{cases} 0 & \frac{\dot{\varepsilon}}{\dot{\varepsilon}_0} < -\frac{\eta}{\bar{k}_v} \\ 1 + \frac{\bar{k}_v}{\eta}\left(\frac{\dot{\varepsilon}}{\dot{\varepsilon}_0}\right) & -\frac{\eta}{\bar{k}_v} \leq \frac{\dot{\varepsilon}}{\dot{\varepsilon}_0} \leq 0 \\ 1 & \frac{\dot{\varepsilon}}{\dot{\varepsilon}_0} > 0 \end{cases} \tag{2}$$

where $\dot{\varepsilon}$ is the fibre contraction / extension strain rate, and the Hill-type constant $\bar{k}_v$ is the fractional reduction in fibre stress upon an increase in shortening strain rate of $\dot{\varepsilon}_0$.

Finite Element Implementation

This active SF formulation [19] (figure 2*a-c*) is implemented into a 3D framework [21] in order to simulate the aforementioned *in vitro* shear experiments. The SF contractility model is implemented in a finite element code (Abaqus Ver. 6.9 (Simulia, RI, USA)) via a user-defined material subroutine. It is important to note that the remodelling and contractility of the actin cytoskeleton is simulated throughout the entire cell cytoplasm, providing a fully predictive active model. At every integration point in the finite element mesh the theoretical framework for SF remodelling and contractility is solved in 240 evenly spaced directions in 3D space. To illustrate this important point, the upper insert in figure 2*d* depicts a point in the cell where an even distribution of SFs is computed in all directions. In contrast, the lower insert depicts a point in the cell where a highly activated SF is computed in one direction, with SFs dissociating in other directions, giving a more aligned fibrous distribution. This simple illustration demonstrates that simulations allow the actin cytoskeleton to actively evolve throughout the entire cell cytoplasm, depending on the signal strength and stress state in the cytoplasm. Hence a full prediction of the distribution of an inhomogeneous anisotropic contractile actin cytoskeleton is provided by this active 3D framework. By integrating the stress over each fibre direction, the active stress tensor is determined. It is important to note that this active framework is placed in parallel with a neo-Hookean hyperelastic formulation [21], which represents the passive non-contractile material (E_{cyto}) surrounding the actin cytoskeleton. A detailed description of the numerical implementation of the active and passive formulation is provided in Appendix B of the Electronic Supplementary Material. The components of the total stress tensor at each integration point in the cytoplasm (figure 2*e*) are given as:

$$\sigma_{ij}^{TOTAL} = \sigma_{ij}^{ACTIVE} + \sigma_{ij}^{PASSIVE} \tag{3}$$

In this study the term cytoplasm refers to the cell body excluding the nucleus. In accordance with Eq. 3, the cytoplasm consists of actively contractile SFs (which make up the actin cytoskeleton) in parallel with a passive non-contractile material (passive cytoplasm), which can be taken to represent microtubules, intermediate filaments, organelles, the cytosol etc.

The nucleus is represented as a passive hyperelastic material. Based on previous studies a Young's modulus of 4 kPa is assumed for the nucleus and a Poisson's ratio of 0.4 is assumed for both the nucleus and the passive cytoplasm material [3, 14, 17]. The substrate and the probe are modelled as rigid bodies, as their materials (glass and tungsten, respectively) are several orders of magnitude stiffer than the cell material. A cohesive zone formulation is used to simulate adhesion between the cell and the substrate [19]. 3D meshes of the cell geometry are based on z-stack images of chondrocytes taken during the *in vitro* experiments. The cell is modelled using 8-noded linear brick elements (C3D8). 3D meshes of the cell geometry were comprised of approximately 80,000 elements. Mesh sensitivity studies were conducted and it was found that increasing the number of elements beyond 80,000 elements did not increase the accuracy of the simulations.

The simulation consists of two steps. During the initial step, the exponentially decaying signal is initiated allowing the formation of SFs in the cell cytoplasm. The step lasts 1000 seconds in order for the SFs to reach an equilibrium state. In the second step, the bottom of the probe is placed 4μm above the substrate and is then moved horizontally towards the cell at a speed of 4μm/s using a constant velocity boundary condition on the top surface of the probe. The computed probe reaction force is plotted against the computed probe indentation for direct comparison with experimental results.

In order to show the average distribution of actin before and during shear, we plot the average SF intensity level ($\bar{\eta}$) at every point in the cytoplasm:

$$\bar{\eta} \equiv \sum_{k=1}^{n} \frac{\eta_k}{n} \tag{4}$$

For direct comparison with the fluorescent microscopy images of chondrocytes labelled for the protein actin, a circular variance (Π) is defined. The circular variance measures the tendency of SFs to bundle in a dominant direction:

$$\Pi = \eta_{max} - \bar{\eta} \tag{5}$$

where η_{max} is the maximum polymerisation level. Π can vary from 0 to 1, corresponding to uniform and perfectly aligned SF distributions, respectively. Contour plots of the circular variance have been shown to correspond to fluorescent or confocal images in which background labelled actin has been removed [20].

Results

A probe force-indentation curve is shown in figure 3*a* for the untreated cell group. The force increases dramatically upon initial probe indentation. A yield point is reached at 34nN, after which the force increases gradually with further indentation. A force of 84nN was measured after 4μm of probe indentation. Disruption of the actin cytoskeleton using cytochalasin-D (cyto-D) results in a markedly different response compared to untreated cells (figure 3*a*). Cyto-D treated chondrocytes did not exhibit a rapid increase in force to a yield point. Instead, a linear force-indentation relationship was observed, with forces being significantly lower than untreated cells at all indentation levels (p<0.05). At 1μm of probe indentation, the mean force for cells treated with cyto-D was approximately six times lower than that for untreated cells.

As shown in figure 3*b*, disruption of the non-contractile components of the cytoskeleton (microtubules and intermediate filaments) results in force-indentation curves that exhibit yield points, similar to that for untreated chondrocytes. For both acrylamide cells (intermediate filaments disrupted) and colchicine cells (microtubules disrupted), measured forces are found to be slightly lower than for untreated cells. However, the yield points for acrylamide and colchicine cells are not statistically different to untreated cells. In contrast, there is a statistical difference between the yield point for cyto-D cells compared to acrylamide and colchicine cells ($p<0.05$). This demonstrates that the distinctive yield point in the probe force-indentation curve occurs due to the contribution of the contractile actin cytoskeleton. A cell height of 11.7 ± 1.2 μm (mean ± SD) was measured experimentally. The nucleus was found to be 1.72 ± 0.38 μm (mean ± SD) above the substrate. No statistical difference was observed between untreated cells and cyto-D, acrylamide or colchicine treated cells in terms of cell and nucleus height.

In order to investigate the biomechanisms underlying the distinctive yield point in the probe force-indentation curve observed experimentally, we simulate the *in vitro* test using the aforementioned active 3D SF framework. The first step of the analysis entails the simulation of SF evolution during seeding of chondrocytes on a rigid (glass) substrate. SF formation is driven by an exponentially decaying signal that initiates at the start of the step. Tension is actively generated by these SFs, which leads to deformation of the cytoplasm. This cytoplasm deformation leads to a shortening of SFs, and an associated tension drop, as described in Eq. 2, which in turn leads to a partial dissociation of the SF.

The predicted evolution of the actin cytoskeleton in response to the exponentially decaying signal is shown at three time-points in figure 4. The mean SF activation level, $\bar{\eta}$, is shown in figure 4*a-c*. A steady state solution is predicted following 1000 seconds, after which no further changes are computed. At this point, the cell is in equilibrium and all SFs in the actin cytoskeleton are at isometric tension with zero fibre strain rate. As can be seen in figure 4*c*, the SF activation level, $\bar{\eta}$, is highest at the base of the cell, as adhesion of the cell to the stiff substrate prevents significant tension reduction in this region of the cytoplasm. Similarly, the stiff nucleus also prevents tension reduction in the surrounding cytoplasm, thus leading to a clustering of the actin cytoskeleton around the nucleus.

As can be seen in figure 4*d-f*, the variance parameter Π shows that SFs are more clustered in a dominant direction at the base of the cell and surrounding the nucleus, following a similar distribution to that of the mean SF activation level $\bar{\eta}$ (figure 4*a-c*). This suggests that SFs are more aligned in a dominant direction at the base of the cell and surrounding the nucleus. However, the maximum value of Π in the cytoplasm is computed as 0.4, suggesting that SF alignment is not pronounced at any point in the cytoplasm.

Figure 5 shows the computed cell deformation at three time-points during probe indentation. The distributions of $\bar{\eta}$ (figure 5*a-c*) and Π (figure 5*d-f*) in the deformed cytoplasm are also shown. Probe indentation leads to a stretching of the cytoplasm at the back of the cell, under the probe (figure 5*b*). The actin cytoskeleton therefore remains in a state of isometric tension with SFs yielding. At the front of the cell the cytoplasm is compressed into the substrate, leading to a shortening of the SFs in the actin cytoskeleton, leading to a reduction in SF tension, in accordance with Eq. 2. This tension drop at the front of the cell leads to dissociation of SFs in this region, in accordance with Eq. 1. Figure 5*b* and *c* illustrate that SF dissociation occurs at the front of the cell during indentation. A similar trend is predicted for the variance (Π), with SF bundles dissociating at the front and yielding at the back of the cell (figure 5*d-f*).

A probe force-indentation curve simulated using the active model is shown in figure 6*a*. A remarkable match with the experimental data for untreated cells is predicted, with an identical yield point being computed. The closest correlation to the untreated cells is achieved

using a maximum SF tension of T_{max}=0.85kPa and a Hill-type constant of $\bar{k}_v$=6, with the rate parameters set to $\dot{\varepsilon}_0$=0.003s^{-1}, θ=70s, k_f =10 and k_b =1. Additionally, the passive Neo-Hookean cytoplasm surrounding the SFs is found to have a Young's modulus of E_{cyto}=1.5kPa. The distinctive yield shape of the experimental and computational probe force-indentation curves can be explained by considering the evolution of SFs in the cell. As previously discussed, SFs at the front of the cell experience reduced tension during shear deformation, leading to dissociation. Therefore, there is a minimal active contribution from the SFs at the front of the cell. At the back of the cell, SFs are stretched and hence yield, producing a constant tension equal to the isometric value. Therefore, the distinctive yield shape of the probe force-indentation curve results from the elongation of SFs at the back of the cell.

When the active SF component of the model is eliminated, leaving just the passive hyperelastic cytoplasm (E_{cyto}=1.5 kPa), the predicted probe force-indentation curve is linear (figure 6*b*) and is extremely similar to the experimentally measured force-indentation curves for cyto-D treated cells. As further highlighted in figure 6*b*, the shape of the force-indentation curve for untreated contractile chondrocytes cannot be simulated by a passive hyperelastic material model. Even if the passive stiffness of the cytoplasm is artificially increased to compute higher probe forces, the resultant "J-type" shape of the force-indentation curve is fundamentally different to the yield-type curve observed experimentally. It is also important to note that significantly different stress distributions are computed in the cytoplasm and cell nucleus for an active and passive cell, as detailed in Appendix C of the Electronic Supplementary Material.

A parametric study of the key material constants that govern the contractile behaviour of SFs (T_{max} and $\bar{k}_v$) is presented in figure 6*c*. It is important to note that the distinctive yield type behaviour is predicted for all values of T_{max}, indicating that the active model is robust in capturing this behaviour. At the lowest level of contractility considered (T_{max}=0.2kPa), a reduced yield point of 8nN is computed, with the probe force-indentation curve slightly higher than the passive hyperelastic probe force-indentation curve (E_{cyto}=1.5kPa in both models). For higher levels of contractility (eg. T_{max}=2kPa), the isometric tension at which SFs are yielding is increased. Therefore, more work is done when SFs at the back of the cell are elongated as the cell deforms, resulting in an increased probe force. For all values of the Hill-type constant ($\bar{k}_v$), a distinctive yielding is predicted. However, the computed yield point is dependent on $\bar{k}_v$, illustrating the importance of the correct calibration of the Hill-type tension velocity relationship for SF contractility during fibre shortening. This parameter has a significant effect on SF tension reduction and hence fibre dissociation at the front of the cell.

The disruption of non-contractile cytoskeletal components is simulated by lowering the passive Young's modulus to E_{cyto}=0.03kPa without changing the active parameters of the model (T_{max}=0.85kPa). Underlying this strategy is an assumption that the treatment of cells with acrylamide or colchicine will alter the mechanical properties of the passive material surrounding the SFs, but will not affect the material properties that govern SF formation and contractility. However, it is important to note that a reduction in the passive stiffness of the cytoplasm will result in a reduced resistance to SF shortening during step one of the analysis. Therefore, a lower steady state distribution of SFs will be computed in response to the exponentially decaying signal. This reduction in SF density in the cytoplasm therefore results in an altered probe force-indentation curve during the second step of the analysis. As shown in figure 6*d*, the reduction of the passive cytoplasm stiffness results in the prediction of slightly lower probe forces than computed for untreated cells with a passive cytoplasm stiffness of to E_{cyto}=1.5kPa (figure 6*a*). Most importantly, the distinctive yield behaviour of the force-indentation curve is not affected by the reduction in passive stiffness. This is due to the regions surrounding the stiff nucleus and at the base of the cell adjacent to the rigid

substrate preventing a reduction in tension despite the lower cytoplasm stiffness. The elongation of SFs in these regions results in the distinctive yield shape of the force-indentation curve.

It is observed in the fluorescent microscopy images (figure 7*a*) that the actin cytoskeleton is uniformly located around the periphery of the base of the cell before shear. A contour plot of the predicted actin cytoskeleton distribution at the base of the cell before shear is plotted in figure 7*b* for comparison with the bottom-up view fluorescence images. The experimental image demonstrates that no distinctive bundling of SFs in a dominant direction occurs, instead the actin cytoskeleton has a smeared appearance. This *in vitro* observation is very close to the predicted distribution using the active model and is mirrored by the low value of Π computed. Following probe indentation, it is observed experimentally that the actin cytoskeleton has dissociated at the front of the cell but it remains intact at the back of the cell (figure 7*c*). The experimentally measured actin intensity at the front of the cell is shown to be significantly lower than in other regions of the cell ($p<0.5$) (See Appendix D in the Electronic Supplementary Material for further details). Again, this correlates very strongly with the active model as shown in figure 7*d*.

Discussion

The current study presents, for the first time, an experimental-computational investigation of the role of the active remodelling and contractility of the actin cytoskeleton in the response of chondrocytes to shear. *In vitro* shear experiments were performed on single chondrocytes, investigating the behaviour both of untreated cells, and of treated cells in which the contractile actin cytoskeleton was removed. A 3D active modelling framework, incorporating signal dependent SF formation and tension-dependent SF dissociation, was used to simulate the *in vitro* experiments. Simulations elucidate the important role of the actin cytoskeleton in chondrocytes during shear deformation. In particular, our study uncovers the following: (i) *in vitro* experiments reveal a distinctive yield shape for the force probe-indentation curve; (ii) in contrast, a linear probe force-indentation curve is observed experimentally for cells in which the active contractile cytoskeleton is removed; (iii) the active modelling framework provides a highly accurate prediction of the response of untreated chondrocytes to shear deformation, capturing the distinctive yield point in the probe force-indentation curve; (iv) a passive hyperelastic model is incapable of predicting the response of untreated chondrocytes during shear, and is only found to provide an accurate prediction for cells in which the actin cytoskeleton has been disrupted; (v) experimentally, disruption of the intermediate filaments and microtubules did not have a significant effect on the response of the cell to shear, with the distinctive yield shape still being observed; (vi) by reducing the passive stiffness of the material that surrounds SFs, the active modelling framework provides an accurate prediction of the behaviour of chondrocytes in which the intermediate filaments and microtubules have been disrupted.

The current study, for the first time, uses a 3D implementation of the active modelling framework to investigate the response of chondrocytes to shear loading. Shear loading is particularly interesting as it imposes both tensile and compressive strain to separate regions within the cell which leads to very different regimes of SF behaviour. The current study demonstrates the importance of firstly predicting where SFs form in the cell, and then the subsequent response of SFs to shear deformation. SF formation is initiated by an exponentially decaying signal within the cell. A steady state equilibrium distribution of the actin cytoskeleton is predicted to occur, with SFs predicted predominantly at the base of the cell and surrounding the stiff nucleus. During subsequent shear deformation, the cytoplasm at the front of the cell is compressed into the substrate, leading to a shortening of SFs in this

region, and as a consequence, tension reduction and localised dissociation is predicted. At the back of the cell, there is no reduction in tension and therefore SFs stretch at isometric tension and remain intact. The yield point in the force-indentation curve is a direct result of the distinctive behaviour of the actin cytoskeleton in compressive and tensile regions of the cell, and can only be predicted by an active modelling framework that incorporates the remodelling and contractility of the actin cytoskeleton. Previous computational models of chondrocytes have relied on passive material formulations [14, 15, 26], ignoring the key biomechanical features underlying SF formation, remodelling, and contractility. A number of previous *in vitro* studies have considered the role of the actin cytoskeleton in chondrocytes in response to mechanical loading. Knight et al. [1] have demonstrated that actin filaments in chondrocytes dynamically adapt to compression and hydrostatic pressure. Additionally, it has been reported that actin filaments contribute significantly to cell stiffness during static compression [27]. It has also been shown that the disruption of the actin cytoskeleton results in a significant reduction in the stiffness of chondrocytes during compression compared to disruption of intermediate filaments and microtubules [7]. The current study, for the first time, provides a quantification and interpretation of the importance of the active contractility of the actin cytoskeleton in chondrocytes during shear.

While the current study highlights the importance of the actin cytoskeleton in the biomechanical behaviour of chondrocytes as discussed above, it is important to note that the actin cytoskeleton is quite smeared in appearance, without distinctive bundling of SFs. This smeared appearance of the chondrocyte actin cytoskeleton is in agreement with previously published *in vitro* images of non-passaged chondrocytes [6, 27, 28], and chondrocytes embedded in an extracellular matrix *in situ* [29, 30]. The active modelling formulation used in the current study has been used to simulate the contractility of smooth muscle cells, mesenchymal stem cells, and fibroblasts seeded on micro-posts [20], and during compression [21]. McGarry et al. [20] determined the maximum isometric tension (T_{max}) for smooth muscle cells (T_{max}=25kPa), mesenchymal stem cells (T_{max}=8kPa), and fibroblasts (T_{max}=3.25kPa). However, these values are much higher than the value calibrated for chondrocytes in the current study (T_{max}=0.85kPa). In the current study simulations predict a low value for SF variance in the chondrocyte cytoplasm ($\Pi_{max}\approx0.4$), indicating that highly aligned SF bundles are not formed for this cell phenotype, which is in agreement with the experimentally observed smeared actin cytoskeleton. In contrast, the SF variance in smooth muscles cells ($\Pi_{max}\approx0.8$), mesenchymal stem cells ($\Pi_{max}\approx0.8$), and fibroblasts ($\Pi_{max}\approx0.8$) is very high, predicting SFs align in dominant directions for these cell phenotypes [21]. However, despite the absence of highly aligned distinctive SFs in chondrocytes, the current study unambiguously demonstrates the significant contribution of the smeared actin cytoskeleton to the biomechanical behaviour of chondrocytes.

The active modelling framework used in the current study provides a prediction of actin cytoskeleton distribution and contractility in chondrocytes, which in turn causes stress in the cell nucleus. Hence, even in the absence of an externally applied load, stresses will be actively generated by the remodelling actin cytoskeleton, as predicted in the first step (prior to probe indentation) of the analyses presented in the current study. In contrast, passive models will not provide a prediction of cell stress generated by a contractile remodelling actin cytoskeleton, hence cytoplasm and nucleus stresses will only be computed in response to an externally applied load. For example, in the current study the stresses computed in the nucleus when using a passive model are entirely due to the indentation of the probe (see Appendix C, Electronic Supplementary Material). It is important to note that following probe indentation, the cytoplasm and nucleus stress state computed using the active SF formulation is considerably different to that computed by the passive cell model. The accurate prediction of nucleus stresses is particularly important in light of *in vitro* studies that have demonstrated

a link between nucleus deformation and gene expression [31, 32]. An experimental study [33] has demonstrated that connections between the cytoskeleton and the nucleus provide a path for signal transfer in cells, and that cellular deformations may lead to changes in DNA structure. Nucleus deformation in chondrocytes has been examined experimentally [34, 35], and simulated using passive material models [36, 37]. The active modelling framework in the current study has the potential to elucidate the link between active contractility, nucleus deformation and mechanotransduction in chondrocytes.

SF dissociation in compressive regions of the cytoplasm is particularly important for chondrocyte mechanotransduction. For instance, the disruption of the actin cytoskeleton in chondrocytes embedded in an agarose gel during cyclic compression has been reported [1, 2]. Such compression induced dissociation of the actin cytoskeleton has important implications for the tissue engineering of cartilage. Shieh and Athanasiou [4] have reported that the dynamic compression of single chondrocytes leads to an upregulation of aggrecan and type II collagen, but static compression causes a downregulation. The findings of the current study can provide an interpretation of previously reported trends for *in vitro* chondrocyte compression experiments. The active modelling framework suggests that cyclic tension reduction, as occurs in dynamic compression experiments, will lead to greater dissociation of the actin cytoskeleton than a single static compression load. The importance of the actin cytoskeleton in the tissue engineering of cartilage is further highlighted by Woods et al. [5] in which chemical disruption of the actin cytoskeleton results in an upregulation of type II collagen and glycosaminoglycans. An application of dynamic boundary conditions to the 3D active modelling framework presented in the current study could potentially identify optimal mechanical loading conditions for the design of tissue-engineered cartilage constructs.

The focus of the current study on shear deformation of single chondrocytes is of particular physiological relevance, given the established links between shear loading and pathological cartilage tissue. Wong and Sah [10] have shown that shear strain is dramatically altered in patellar cartilage due to focal defects. In addition, shear strain is significantly increased in degenerated cartilage and this outcome is amplified with reduced lubrication [38]. Smith et al. [39] have demonstrated that shear stress decreases aggrecan and collagen type II expression in osteoarthritic chondrocytes. Additionally, shear stress causes an increase in nitric oxide production in osteoarthritic chondrocytes leading to increased cell apoptosis [40]. The effect of altered shear strains due to focal defects or deteriorated tissue on cytoskeleton remodelling and contractility in chondrocytes *in situ* is the subject of a follow-on investigation.

In the current study, results are presented only for probe indentations that did not lead to bond rupture between the cell and the substrate. The absence of bond rupture was confirmed by fluorescent imaging of the focal adhesion protein vinculin, which was observed at the periphery of the cell. Previous *in vitro* experiments have investigated cell adhesion and detachment during shear deformation [13, 41]. A computational study [17], based on the experimental findings of Huang et al [13], illustrates that a strengthening of the cell-substrate interface in tandem with cytoplasm stiffening during cell spreading results in increased cell detachment forces. Experimentally, it has been demonstrated that focal adhesion formation is sensitive to external mechanical stimulation [42]. Also, the relationship between focal adhesion area and active cell contractility has been reported [43]. Following from the experiments presented in the current study and those of Huang et al. [13], a series of *in vitro* tests should be performed in which focal adhesion evolution is examined as a function of probe indentation and actin cytoskeletal contractility. This would provide insight into the important link between the formation of focal adhesions and tractions at the cell-extracellular matrix interface due to internal contractility and external applied loading.

In conclusion, this study illustrates the importance of the actin cytoskeleton in the shear deformation of chondrocytes. *In vitro* shearing of single cells reveals a characteristic yield point in the force-indentation curve for untreated chondrocytes. Simulations using an active 3D framework for SF remodelling and contractility reveal for the first time the importance of the actin cytoskeleton in the biomechanics of chondrocytes. The distinctive force-indentation curve results from the yielding of the SFs in localised tensile regions at the back of the cell, in tandem with the dissociation of SFs in localised compressive regions at the front of the cell. Importantly, *in vitro* disruption of the actin cytoskeleton results in a linear force-indentation relationship, in contrast to the yield-type relationship observed for untreated chondrocytes. It is demonstrated that passive hyperelastic cell models can only be used to predict the response of non-contractile cells to shear deformation. The present study demonstrates that the simulation of the active cellular biomechanisms is critical in order to provide accurate predictions of the response of cells to mechanical stimuli. Furthermore, the current study presents, for the first time, a novel computational-experimental methodology for the calibration of the active model in which active and passive cell behaviour has been parsed. The combined modelling-experimental framework uncovers the contribution of active contractility and remodelling of the actin cytoskeleton to the response of chondrocytes to shear loading, with important implications for the understanding of the pathogenesis of cartilage tissue and the tissue engineering of cartilage constructs.

Acknowledgements
Funding support was provided by the Irish Research Council for Science, Engineering and Technology (IRCSET) postgraduate scholarship under the EMBARK initiative, and by the Science Foundation Ireland Research Frontiers Programme (SFI-RFP/ENM1726) and Short Term Travel Fellowship (SFI-STTF). The authors wish to acknowledge the SFI/HEA Irish Centre for High-End Computing (ICHEC) for the provision of computational facilities and support.

References

1. Knight, M. M., Toyoda, T., Lee, D. A., & Bader, D. L., 2006 Mechanical compression and hydrostatic pressure induce reversible changes in actin cytoskeletal organisation in chondrocytes in agarose. *J Biomech* **39**, 1547-1551.
2. Campbell, J. J., Blain, E. J., Chowdhury, T. T., & Knight, M. M., 2007 Loading alters actin dynamics and up-regulates cofilin gene expression in chondrocytes. *Biochem Biophys Res Commun* **361**, 329-334.
3. Leipzig, N. D. & Athanasiou, K. A., 2008 Static compression of single chondrocytes catabolically modifies single-cell gene expression. *Biophysical journal* **94**, 2412-2422.
4. Shieh, A. C. & Athanasiou, K. A., 2007 Dynamic compression of single cells. *Osteoarthr Cartilage* **15**, 328-334.
5. Woods, A., Wang, G., & Beier, F., 2007 Regulation of chondrocyte differentiation by the actin cytoskeleton and adhesive interactions. *Journal of cellular physiology* **213**, 1-8.
6. Trickey, W. R., Vail, T. P., & Guilak, F., 2004 The role of the cytoskeleton in the viscoelastic properties of human articular chondrocytes. *J Orthop Res* **22**, 131-139.
7. Ofek, G., Wiltz, D. C., & Athanasiou, K. A., 2009 Contribution of the cytoskeleton to the compressive properties and recovery behavior of single cells. *Biophys J* **97**, 1873-1882.
8. Buckley, M. R., Gleghorn, J. P., Bonassar, L. J., & Cohen, I., 2008 Mapping the depth dependence of shear properties in articular cartilage. *J Biomech* **41**, 2430-2437.
9. Wong, B. L. & Sah, R. L., 2010 Mechanical asymmetry during articulation of tibial and femoral cartilages: Local and overall compressive and shear deformation and properties. *J Biomech* **43**, 1689-1695.
10. Wong, B. L. & Sah, R. L., 2010 Effect of a focal articular defect on cartilage deformation during patello-femoral articulation. *J Orthop Res* **28**, 1554-1561.
11. Sawae, Y., Shelton, J. C., Bader, D. L., & Knight, M. M., 2004 Confocal analysis of local and cellular strains in chondrocyte-agarose constructs subjected to mechanical shear. *Ann Biomed Eng* **32**, 860-870.
12. Smith, R. L., Trindade, M., Ikenoue, T., Mohtai, M., Das, P., Carter, D., Goodman, S., & Schurman, D., 2000 Effects of shear stress on articular chondrocyte metabolism. *Biorheology* **37**, 95-108.
13. Huang, W., Bahman, A. J. H., Torres, R., Lebaron, G., & Athanasiou, K. A., 2003 Temporal effects of cell adhesion on mechanical characteristics of the single chondrocyte. *J Orthop Res* **21**, 88-95.
14. Ofek, G., Natoli, R. M., & Athanasiou, K. A., 2009 In situ mechanical properties of the chondrocyte cytoplasm and nucleus. *J Biomech* **42**, 873-877.
15. Baaijens, F. P. T., Trickey, W. R., Laursen, T. A., & Guilak, F., 2005 Large deformation finite element analysis of micropipette aspiration to determine the mechanical properties of the chondrocyte. *Ann Biomed Eng* **33**, 494-501.
16. Trickey, W. R., Baaijens, F. P. T., Laursen, T. A., Alexopoulos, L. G., & Guilak, F., 2006 Determination of the poisson's ratio of the cell: Recovery properties of chondrocytes after release from complete micropipette aspiration. *J Biomech* **39**, 78-87.
17. McGarry, J. P. & McHugh, P. E., 2008 Modelling of in vitro chondrocyte detachment. *J Mech Phys Solids* **56**, 1554-1565.
18. McGarry, J. P., 2009 Characterization of cell mechanical properties by computational modeling of parallel plate compression. *Ann Biomed Eng* **37**, 2317-2325.

19. Deshpande, V. S., McMeeking, R. M., & Evans, A. G., 2006 A bio-chemo-mechanical model for cell contractility. *Proc Natl Acad Sci* **103**, 14015.
20. McGarry, J. P., Fu, J., Yang, M. T., Chen, C. S., McMeeking, R. M., Evans, A. G., & Deshpande, V. S., 2009 Simulation of the contractile response of cells on an array of micro-posts. *Philos Trans R Soc, A* **367**, 3477.
21. Ronan, W., Deshpande, V., McMeeking, R. M., & McGarry, J. P., 2012 Numerical investigation of the active role of the cytoskeleton in the compression resistance of cells. *J Mech Behav Biomed Mater* **accepted.**
22. Ofek, G., Dowling, E. P., Raphael, R. M., McGarry, J. P., & Athanasiou, K. A., 2009 Biomechanics of single chondrocytes under direct shear. *Biomechanics and modeling in mechanobiology* **9**, 153-162.
23. Burridge, K. & Chrzanowska-Wodnicka, M., 1996 Focal adhesions, contractility, and signaling. *Annual review of cell and developmental biology* **12**, 463-518.
24. Roberts, S. R., Knight, M. M., Lee, D. A., & Bader, D. L., 2001 Mechanical compression influences intracellular ca2+ signaling in chondrocytes seeded in agarose constructs. *J Appl Physiol* **90**, 1385-1391.
25. Hill, A. V., 1938 The heat of shortening and the dynamic constants of muscle. *Proc R Soc London, Ser B* **126**, 136-195.
26. Nguyen, B. V., Wang, Q. G., Kuiper, N. J., El Haj, A. J., Thomas, C. R., & Zhang, Z., 2010 Biomechanical properties of single chondrocytes and chondrons determined by micromanipulation and finite-element modelling. *J R Soc Interface* **7**, 1723-1733.
27. Leipzig, N. D., Eleswarapu, S. V., & Athanasiou, K. A., 2006 The effects of tgf-[beta]1 and igf-i on the biomechanics and cytoskeleton of single chondrocytes. *Osteoarthr Cartilage* **14**, 1227-1236.
28. Idowu, B. D., Knight, M. M., Bader, D. L., & Lee, D. A., 2000 Confocal analysis of cytoskeletal organisation within isolated chondrocyte sub-populations cultured in agarose. *Histochem J* **32**, 165-174.
29. Durrant, L., Archer, C., Benjamin, M., & Ralphs, J., 1999 Organisation of the chondrocyte cytoskeleton and its response to changing mechanical conditions in organ culture. *J Anat* **194**, 343-353.
30. Langelier, E., Suetterlin, R., Hoemann, C. D., Aebi, U., & Buschmann, M. D., 2000 The chondrocyte cytoskeleton in mature articular cartilage: Structure and distribution of actin, tubulin, and vimentin filaments. *J Histochem Cytochem* **48**, 1307.
31. Roca-Cusachs, P., Alcaraz, J., Sunyer, R., Samitier, J., Farre, R., & Navajas, D., 2008 Micropatterning of single endothelial cell shape reveals a tight coupling between nuclear volume in g1 and proliferation. *Biophysical journal* **94**, 4984-4995.
32. Thomas, C. H., Collier, J. H., Sfeir, C. S., & Healy, K. E., 2002 Engineering gene expression and protein synthesis by modulation of nuclear shape. *Proc Natl Acad Sci* **99**, 1972.
33. Maniotis, A. J., Chen, C. S., & Ingber, D. E., 1997 Demonstration of mechanical connections between integrins, cytoskeletal filaments, and nucleoplasm that stabilize nuclear structure. *Proc Natl Acad Sci* **94**, 849.
34. Guilak, F., 1995 Compression-induced changes in the shape and volume of the chondrocyte nucleus. *J Biomech* **28**, 1529-1541.
35. Guilak, F., Tedrow, J. R., & Burgkart, R., 2000 Viscoelastic properties of the cell nucleus. *Biochem Biophys Res Commun* **269**, 781-786.
36. Finan, J. D., Chalut, K. J., Wax, A., & Guilak, F., 2009 Nonlinear osmotic properties of the cell nucleus. *Annals of biomedical engineering* **37**, 477-491.
37. Vaziri, A. & Mofrad, M. R. K., 2007 Mechanics and deformation of the nucleus in micropipette aspiration experiment. *J Biomech* **40**, 2053-2062.

38. Wong, B. L., Bae, W. C., Chun, J., Gratz, K. R., Lotz, M., & Sah, R. L., 2008 Biomechanics of cartilage articulation: Effects of lubrication and degeneration on shear deformation. *Arthritis Rheum* **58**, 2065-2074.
39. Smith, R. L., Carter, D. R., & Schurman, D. J., 2004 Pressure and shear differentially alter human articular chondrocyte metabolism: A review. *Clin Orthop Relat Res*, S89-95.
40. Lee, M. S., Trindade, M. C. D., Ikenoue, T., Schurman, D. J., Goodman, S. B., & Smith, R. L., 2002 Effects of shear stress on nitric oxide and matrix protein gene expression in human osteoarthritic chondrocytes in vitro. *J Orthop Res* **20**, 556-561.
41. Hoben, G., Huang, W., Thoma, B. S., LeBaron, R. G., & Athanasiou, K. A., 2002 Quantification of varying adhesion levels in chondrocytes using the cytodetacher. *Ann Biomed Eng* **30**, 703-712.
42. Sniadecki, N. J., Anguelouch, A., Yang, M. T., Lamb, C. M., Liu, Z., Kirschner, S. B., Liu, Y., Reich, D. H., & Chen, C. S., 2007 Magnetic microposts as an approach to apply forces to living cells. *Proc Natl Acad Sci* **104**, 14553.
43. Tan, J. L., Tien, J., Pirone, D. M., Gray, D. S., Bhadriraju, K., & Chen, C. S., 2003 Cells lying on a bed of microneedles: An approach to isolate mechanical force. *Proc Natl Acad Sci* **100**, 1484-1489.

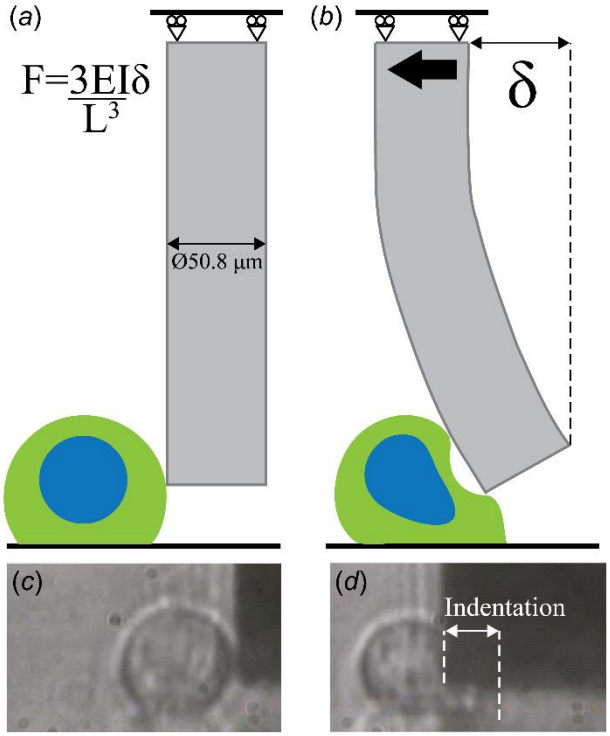

Figure 1

Schematic image of cell and probe: (*a*) prior to indentation; (*b*) during shear indentation. Experimental image of cell and probe: (*c*) prior to indentation; (*d*) during shear indentation. (Note: probe and deflection δ are not to scale in (*a*) and (*b*)).

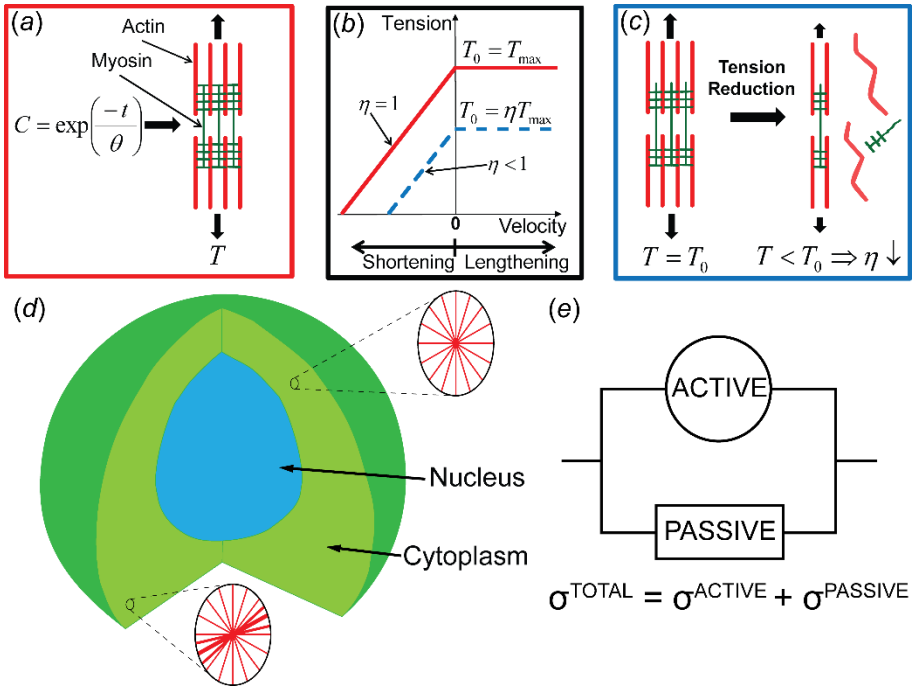

Figure 2

(*a*) SF formation in response to an exponentially decaying signal *C*, and generating tension *T*; (*b*) cross-bridge cycling tension-velocity relationship for SFs. The red solid curve corresponds to a fully activated SF. The blue dashed curve corresponds to a SF that has partially dissociated ($0 < \eta > 1$); (*c*) SF dissociation in response to tension reduction; (*d*) Cut away view of a 3D cell and nucleus geometry. Insets show schematic of SF distribution on 2D sections at two points in the cell cytoplasm for illustrative purposes (note: distribution is actually predicted in 3D space at every integration point in the cell cytoplasm); (*e*) the active SF and passive components of the model are placed in parallel and summed to give the total stress.

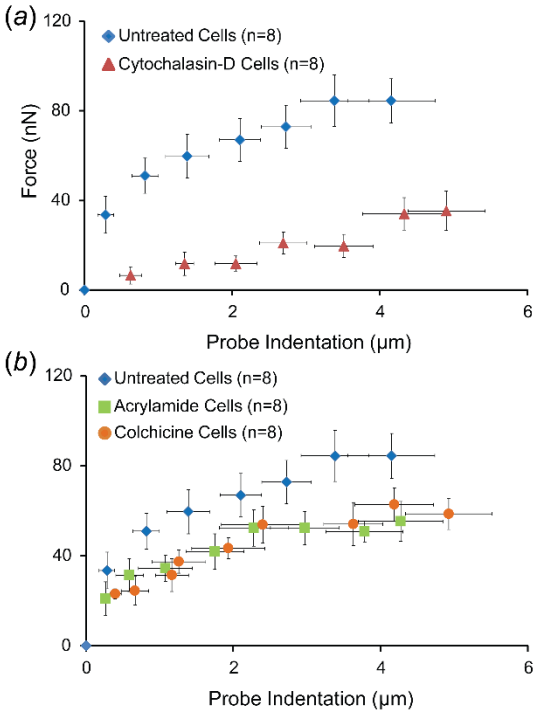

Figure 3

Experimental probe force-indentation data for: (*a*) untreated and cyto-D cells; (*b*) untreated, acrylamide and colchicine cells. The data points represent the average force and indentation values for the experimental groups (mean ± SD).

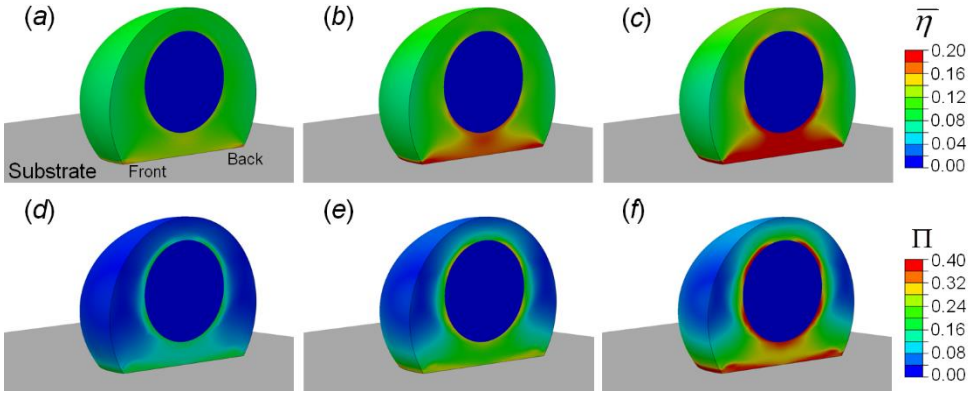

Figure 4

Contour plots of the average SF activation levels ($\bar{\eta}$): (*a*) at 30s after signal initiation; (*b*) at 70s after signal initiation; (*c*) at 1000s after signal initiation. Contour plots of the variance (Π): (*d*) at 30s after signal initiation; (*e*) at 70s after signal initiation; (*f*) at 1000s after signal initiation. A half cell is shown due to symmetry.

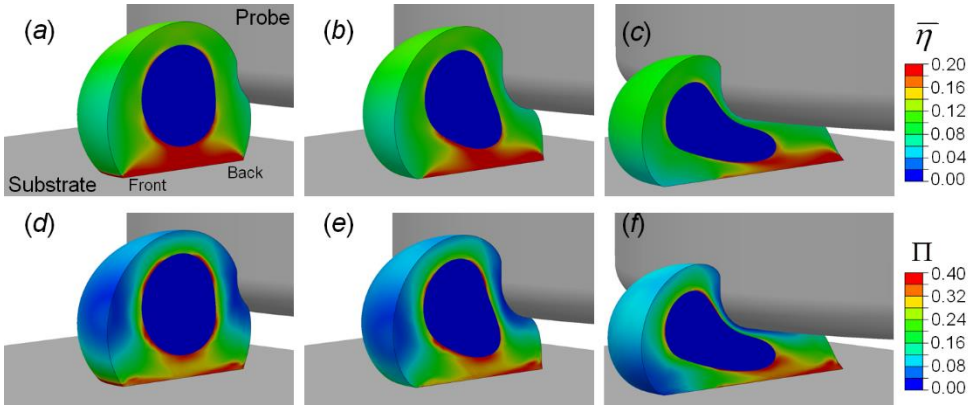

Figure 5

Contour plots of the average SF activation levels ($\bar{\eta}$) at a probe indentation of: (*a*) 1.5μm; (*b*) 4.7μm; (*c*) 10.9μm. Contour plots of the variance (Π) at a probe indentation of: (*d*) 1.5μm; (*e*) 4.7μm; (*f*) 10.9μm. A half cell is shown due to symmetry.

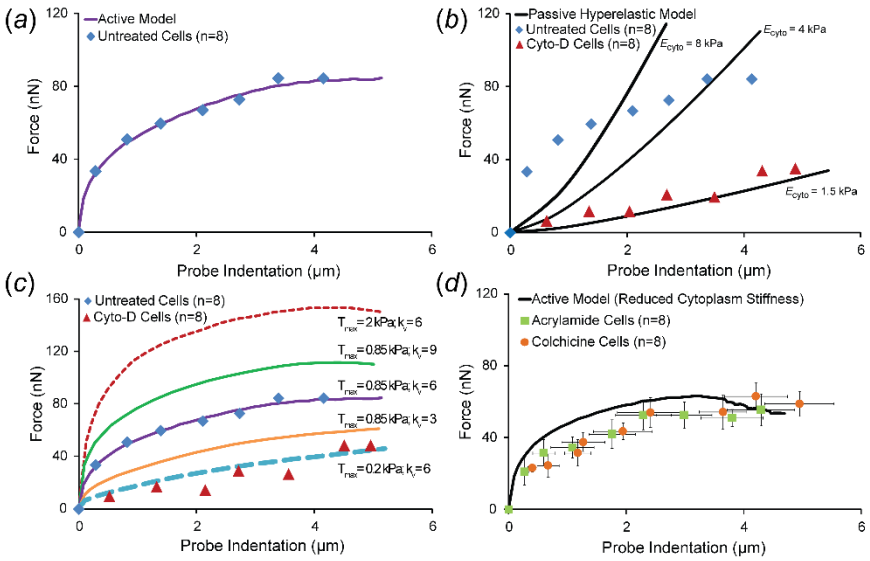

Figure 6

(*a*) Computational probe force-indentation curves for the active model (E_{cyto}=1.5kPa, T_{max}=0.85kPa, $\bar{k}_v$ =6), mean experimental untreated cell data included for comparison. (*b*) Computational force probe-indentation curves assuming a passive hyperelastic cell cytoplasm. Predictions are shown for three values of cytoplasm stiffness: 1.5kPa, 4kPa, and 8kPa. (*c*) Parametric study of the effect of active parameters T_{max} and $\bar{k}_v$ on predicted probe force-indentation curves (with E_{cyto}=1.5kPa). (*d*) Computational probe force-indentation curve for the active model with reduced cytoplasm stiffness (E_{cyto}=0.03kPa, T_{max}=0.85kPa, $\bar{k}_v$ =6), and experimental probe force-indentation data (mean ± SD) for acrylamide and colchicine treated cells.

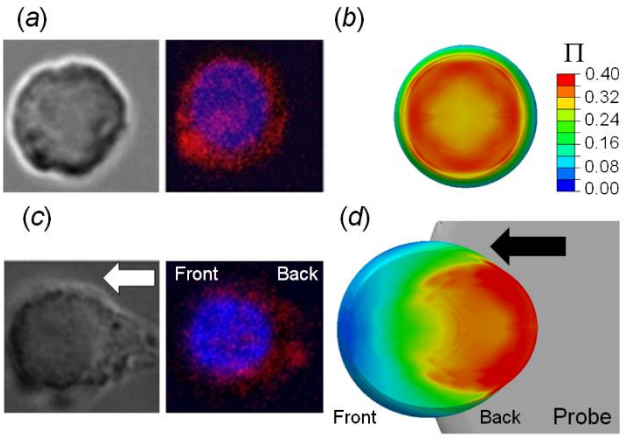

Figure 7

(*a*) Representative brightfield and fluorescent image (bottom-up view) of a cell before shear deformation, with nuclei (blue) and actin (red) shown at a focal plane near the base; (*b*) Predicted distribution of the actin cytoskeleton before shear deformation for the active model (E_{cyto}=1.5kPa, T_{max}=0.85kPa, $\bar{k}_v$ =6); (*c*) Representative brightfield and fluorescent image (bottom-up view) of a cell after shear deformation; (*d*) Predicted distribution of the actin cytoskeleton following 10.9μm of probe indentation. The arrow indicates the direction of probe movement.